

# Journal Pre-proof

Ferulin C triggers potent PAK1 and p21-mediated anti-tumor effects in breast cancer by inhibiting Tubulin polymerization *in vitro* and *in vivo*

Dahong Yao, Dabo Pan, Yongqi Zhen, Jian Huang, Jinhui Wang, Jin Zhang, Zhendan He



PII: S1043-6618(19)32086-9  
DOI: <https://doi.org/10.1016/j.phrs.2019.104605>  
Reference: YPHRS 104605

To appear in: *Pharmacological Research*

Received Date: 24 September 2019  
Revised Date: 24 November 2019  
Accepted Date: 13 December 2019

Please cite this article as: Yao D, Pan D, Zhen Y, Huang J, Wang J, Zhang J, He Z, Ferulin C triggers potent PAK1 and p21-mediated anti-tumor effects in breast cancer by inhibiting Tubulin polymerization *in vitro* and *in vivo*, *Pharmacological Research* (2019), doi: <https://doi.org/10.1016/j.phrs.2019.104605>

This is a PDF file of an article that has undergone enhancements after acceptance, such as the addition of a cover page and metadata, and formatting for readability, but it is not yet the definitive version of record. This version will undergo additional copyediting, typesetting and review before it is published in its final form, but we are providing this version to give early visibility of the article. Please note that, during the production process, errors may be discovered which could affect the content, and all legal disclaimers that apply to the journal pertain.

© 2019 Published by Elsevier.

## Ferulin C triggers potent PAK1 and p21-mediated anti-tumor effects in breast cancer by inhibiting Tubulin polymerization *in vitro* and *in vivo*

Dahong Yao<sup>1</sup>, Dabo Pan<sup>3</sup>, Yongqi Zhen<sup>2</sup>, Jian Huang<sup>4,5</sup>, Jinhui Wang<sup>4,5\*</sup>, Jin Zhang<sup>2\*</sup>, Zhendan He<sup>1\*</sup>

<sup>1</sup>School of Pharmaceutical Sciences, Guangdong Key Laboratory for Genome Stability & Human Disease Prevention, Shenzhen Key Laboratory of Novel Natural Health Care Products, Innovation Platform for Natural small molecule Drugs, Engineering Laboratory of Shenzhen Natural small molecule Innovative Drugs, Shenzhen University, Shenzhen 518060, China.

<sup>2</sup>State Key Laboratory of Biotherapy and Cancer Center, West China Hospital, Sichuan University, and Collaborative Innovation Center for Biotherapy, Chengdu 610041, China

<sup>3</sup>Institute of Traditional Chinese Medicine & Natural Products, and Guangdong Province Key Laboratory of Pharmacodynamic Constituents of TCM and New Drugs Research, College of Pharmacy, Jinan University, Guangzhou 510632, P. R. China

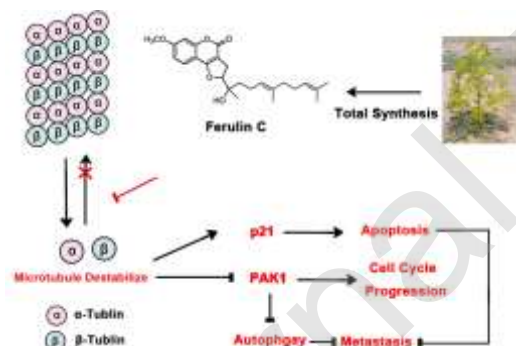
<sup>4</sup>Shenzhen Honghui Bio-Pharmaceutical Co. Ltd., Shenzhen 518118, China

<sup>5</sup>College of Pharmacy, Harbin Medical University, Harbin 150081, China

### Corresponding Author:

Jin Zhang, E-mail: jinjinlovemama@163.com; Zhendan He, E-mail: hezhendan@126.com

### Graphical abstract



### Highlights:

- Ferulin C was documented to impede the tubulin polymerization through binding to the Colchicine site of tubulin, resulting in microtubule destabilization.
- Ferulin C stimulates significant cell cycle arrest, profound cell apoptosis and cell migration.
- The inhibition of PAK1 impaired the Raf-MEK1/2-ERK1/2 and CHK2-CDC25A signaling, resulting in inhibiting cell proliferation and metastasis.

**Abstract**

Ferulin C, a natural sesquiterpene coumarin, isolated from the roots of *Ferula ferulaeoides* (Steud.) Korov, displaying potent antiproliferatory activity against breast cancer cells. This study aimed to elucidate the underlying molecular mechanisms of Ferulin C-induced breast cancer cells death *in vitro* and *in vivo*. Ferulin C presented potent antiproliferatory activity against MCF-7 and MDA-MB-231 cells and remarkable tubulin polymerization inhibitory activity ( $IC_{50} = 9.2 \mu\text{M}$ ). Meanwhile, we predicted Ferulin C bind to the Colchicine site of tubulin through CETSA assay, molecular docking and molecular dynamics (MD) simulations. In immunofluorescence assay, Ferulin C disturbed the microtubule integrity and structure. Furthermore, Ferulin C stimulated significant cell cycle arrest in the G1/S period via p21<sup>Cip1/Waf1</sup> - CDK2 signaling, induced classic cell apoptosis, impaired metastasis via down-regulating Ras-Raf-ERK and AKT-mTOR signaling. Intriguingly, Ferulin C treatment induced autophagy by ULK1 signaling to synergize with the inhibition of proliferation and metastasis. Based upon the RNAseq analysis, PAK1, as a novel essential modulator, was involved in the signaling regulated by Ferulin C - induced  $\alpha/\beta$ -tubulin depolymerization. Additionally, Ferulin C displayed an acceptable antiproliferatory activity in an MCF-7 xenograft model without inducing obvious weight loss in the Ferulin C treated mice. Summarily, our findings substantiated that Ferulin C was a potent, colchicine site binding microtubule-destabilizing agent with anti-proliferation and anti-metastasis activity via PAK1 and p21-mediated signaling in breast cancer cells.

**Key words:** Ferulin C, tubulin polymerization, breast cancer, apoptosis, autophagy, metastasis.

**Abbreviations**

MDAs, Microtubule destabilizing agents; JNK, c-Jun N-terminal kinase; VEGF, vascular endothelial growth factor; VEGFR2, Vascular Endothelial Growth Factor Receptor2; ULK1, unc-51 like autophagy activating kinase 1; ATG5, Autophagy protein 5; ATG12, Autophagy protein 12; PAK1, p21 activated kinase 1; MTT, methyl thiazolyl tetrazolium; MD, molecular dynamic; CDK2, cyclin-dependent kinase 2; Bax, BCL2-Associated X Protein; PARP, poly ADP-ribose polymerase; Ras, GTPase HRas; MEK, ERK, extracellular regulated protein kinases; AKT,

Protein kinase B; mTOR, Mammalian Target of Rapamycin; LC3, Microtubule-Associated Protein-Light Chain 3p; Bcl-2, B-cell lymphoma 2; 3-MA, 3-Methyladenine; PPI, protein-protein interactions; GO, Gene Ontology; TCGA, The Cancer Genome Atlas; CHK2, Checkpoint kinase 2; Beclin-1, Coiled-Coil, Myosin-like BCL2 Interacting Protein; Caspase, Cysteine Aspartate-Specific Protease; DMSO, Dimethyl Sulfoxide.

## 1. INTRODUCTION

*Ferula ferulaeoides* is one of the genus *Ferula* species, reported to exhibit a variety of pharmacological activities, including anti-spasmodic, hypotensive, anti-carcinogenic, anti-coagulant and anti-inflammatory [1]. In our previous studies, Ferulin C, sesquiterpene coumarin, was isolated from the ethyl acetate layer extract of *Ferula* genus, displaying diverse inhibitory activity in cancer cell lines. Breast cancer is one of the most common malignancies in women, causing accumulating deaths over the world [2]. Microtubule inhibitors from natural products have emerged as one of the most intensive classes of drugs for cancer therapy [3]. Microtubules play an essential role in the development, maintenance of cell shape, cell signaling, cell mitosis and division [4]. Microtubule destabilizing agents (MDAs) could induce destabilization of microtubule to block microtubule assemblies, such as Vinca alkaloids and Colchicine [5, 6]. In recent years, accumulating researches reported that Microtubule destabilizing agents elicited multiple biological effects including apoptosis, cell cycle, metastasis, and autophagy. YSL-12 as a microtubule-destabilizing agent, which presented potent cytotoxicity against human cancer cell lines, could induce cell cycle arrest in the G2/M phase and stimulate cell apoptosis in a concentration-dependent manner [7]. MT189 could suppress proliferation, migration, and differentiation (tube formation) of vascular endothelial cells, which are very critical steps in angiogenesis, resulting in inhibiting angiogenesis *via* JNK activation and subsequent inhibition of the VEGF/VEGFR2 signaling axis [8]. Some ATG proteins, such as Beclin 1, ULK1, ATG5 and ATG12, are involved in the early steps of autophagosome formation are enriched in the dynamic MT fraction, which suggested that the dynamic subset of MTs supports the assembly of pre-autophagosomal structures [9]. Collectively, Microtubule destabilizing agents (MDAs) could regulate the process of cell proliferation, apoptosis, metastasis, *etc.*, but the detailed mediated mechanisms still remains unclear, which dramatically impeded the efforts to facilitate

the proper and rational use of microtubule inhibitors for cancer therapy.

In this study, the total synthesis of Ferulin C was reported in detail for the first time. Furthermore, we unveiled that Ferulin C, as a novel microtubule destabilizing agent, stimulated significant cell cycle arrest at the G1/S period, induced cell apoptosis, and inhibited metastasis via Ras-Raf-ERK and AKT-mTOR signalling pathway suppression. Ferulin C also elicited autophagy associated cell death to synergize with the proliferation and metastasis in MCF-7 and MDA-MB-231 cells. PAK1 was identified as a novel essential modulator involved in the signaling regulated by Ferulin C -induced  $\alpha/\beta$ -tubulin depolymerization. Taken together, our data demonstrated Ferulin C as a potent, colchicine site binding, microtubule-destabilizing agent with potent anti-proliferation and anti-metastasis activity via PAK1 and p21-mediated signaling in breast cancer cells. Additionally, the *in vivo* assay demonstrated the acceptable anti-tumor effect of Ferulin C. These findings highlighted a novel potent microtubule destabilizing agent, shed light on the detailed mechanisms involved in apoptosis and autophagy induced by Tubulin polymerization inhibition and provided a rationale for the development of natural products.

## 2. MATERIALS AND METHODS

### 2.1 Cell culture, antibodies and reagents

MCF-7 cells and MDA-MB-231 cells were cultured in DMEM with 10% fetal bovine serum and incubated with 5% CO<sub>2</sub>. Antibodies used in this study were as follows: p21<sup>Waf1/Cip1</sup> (2947, CST), CDK2 (2546, CST), p-CDK2<sup>Thr160</sup> (2561, CST), Cyclin E1 (4129, CST), p-Cyclin E1<sup>Thr77</sup> (ab124696, abcam), 14-3-3 (8312, CST), Bcl-2 (15071, CST), caspase8 (9746, CST), Cleaved-caspase7 (8438, CST), Caspase 9 (ab115792, abcam), MMP-2 (40994, CST), LC3B (3868, CST), p62 (5114, CST), E-cadherin (14472, CST), PARP (9532, CST), caspase-3 (9665, CST), Bax (5023, CST), c-Raf (53745, CST), p-c-Raf Ser259 (9421, CST), p-c-Raf<sup>Ser338</sup> (9427, CST), MEK (4694, CST), ERK (9102, CST), p-ERK Thr202/Tyr204 (9101, CST), AKT (4691, CST), p-AKT<sup>Ser473</sup> (4060, CST), mTOR (2983, CST), p-mTOR<sup>Ser2448</sup> (5536, CST), ULK1 (6439, CST), p-ULK1<sup>Ser555</sup> (5869, CST), PAK1 (2602, CST), CHK2 (6334, CST), Ras (3339, CST), CDC25A (3652, CST), p-CDC25A<sup>Ser124</sup> (ab156574, abcam), Beclin1 (4122, CST), p-MEK<sup>Ser217/221</sup> (9154, CST), Ambra1 (24907, CST), b-actin (3700, CST). The plasmid encoding un-tagged constitutively PAK1,  $\beta$ -tubulin and mock vector plasmid were purchased from Sino Biological (Beijing, China).

## 2.2 Cell viability assay

Cell viability was measured by the MTT assay [10]. Cells were dispensed in 96-well plates at a density of  $5 \times 10^4$  cells/ml. After 24 h incubation, cells were treated with different concentrations of compounds for the indicated periods.

## 2.3 The target prediction of Ferulin C

The target prediction of Ferulin C was performed through pharmacophore-based parallel screening by Pipeline Pilot-based program protocol included in Discovery Studio 3.5 (Accelrys; SciTegic). The pharmacophore database was collected and modified from the scPDB database (<http://bioinfo-pharma.u-strasbg.fr/scPDB>) [11]. The docking program was used LibDock protocol and the default value was adopted.

## 2.4 Molecular docking

The discovery Studio 3.5 was used to perform molecular docking of compound Ferulin C within the  $\beta$ -tubulin (PDB code 4o2a) downloaded from PDB databank (<https://www.rcsb.org>) [12]. The active binding site was defined according to the Colchicine binding site with a radius of 9.5 Å. The protein structure was processed by adding hydrogen atoms, removing water, and assigning Charmm forcefield. The gold score was selected as the score function, and the other parameters were set as default. A maximum of 20 conformations was generated. 30 ligand poses were allowed to be saved with a minimum RMSD between final poses of 0.50 Å.

## 2.5 Molecular dynamics (MD) simulations

The MD simulation was performed by Amber 10 package [13]. The first restraining energy minimization was carried out by the steepest descent method with 0.1 kcal/mol·Å<sup>2</sup> restraints for all atoms of the complexes for 5000 steps. And then, we removed the restraints of ligand (only restraining the protein) to perform the second energy minimization, and another energy minimization was made under releasing all the restraints. 5000 steps were set for each energy minimization. To handle the long-range Coulombic interactions, the particle mesh Ewald (PME) summation was used. The SHAKE algorithm was employed on all atoms covalently bonded to a hydrogen atom, allowing for an integration time step of 2 fs in the equilibration and subsequent production runs. The annealed program was from 0 to 310 K for 50 ps. Under releasing all the restraints, the system was again equilibrated for 500 ps. The production phase of the simulations was run without any restraints for a total of 70 ns.

## 2.6 Binding free energy calculation (MM-GBSA)

MM-GBSA calculation was performed using AMBER10 [13]. First, we performed the generation of multiple snapshots from an MD trajectory of the protein-ligand complex, stripped of water molecules and counter ions. Snapshots were extracted from the equilibration section of MD trajectory with equally spaced at 10 ps intervals. For each snapshot, the free energy is calculated for each molecular species (complex, protein, and ligand). The binding free energy is computed as

$$\Delta G_{bind} = G_{complex} - G_{protein} - G_{ligand}$$

The free energy,  $G$ , for each species can be calculated by the following scheme using the MM-GBSA method:

$$G = E_{gas} + G_{sol} - TS$$

$$E_{gas} = E_{int} + E_{ele} + E_{vdw}$$

$$E_{int} = E_{bond} + E_{angle} + E_{torsion}$$

$$G_{sol} = G_{GB} + G_{nonpolar}$$

$$G_{nonpolar} = \gamma SAS$$

$E_{gas}$  is the gas-phase energy;  $E_{int}$  is the internal energy;  $E_{bond}$ ,  $E_{angle}$ , and  $E_{torsion}$  are the bond, angle, and torsion energies, respectively; and  $E_{ele}$  and  $E_{vdw}$  are the Coulomb and van der Waals energies, respectively.  $E_{gas}$  was calculated using the AMBER molecular mechanics force field.  $G_{sol}$  is the solvation free energy and can be decomposed into polar and nonpolar contributions.  $G_{GB}$  is the polar solvation contribution calculated by solving the GB equation. The dielectric constant of solvent and solute were set to 80 and 1, respectively.  $G_{nonpolar}$  is the nonpolar solvation contribution and was estimated by the solvent-accessible surface area (SAS) determined using a water probe radius of 1.4 Å. The surface tension constant  $\gamma$  was set to 0.0072 kcal/mol/Å<sup>2</sup> [14].

## 2.7 Tubulin Polymerization Assay

Microtubule protein was isolated by three cycles of temperature-dependent assembly/disassembly according to Shelanski *et al* [15] in 100 mM PIPES (pH 6.5), 1 mM MgSO<sub>4</sub>, 2 mM EGTA, 1 mM GTP and 1 mM 2-mercaptoethanol. In the first cycle of polymerization, glycerol and phenylmethylsulfonyl fluoride were added to 4 M and 0.2 mM, respectively. Homogeneous tubulin was prepared from microtubule protein by phosphocellulose (P11) chromatography as described 28. The purified proteins were stored in

aliquots at  $-70^{\circ}\text{C}$ . Tubulin protein was mixed with different concentrations of compound in PEM buffer (100 mM PIPES, 1 mM  $\text{MgCl}_2$ , and 1 mM EGTA) containing 1 mM GTP and 5 % glycerol. Microtubule polymerization was monitored at  $37^{\circ}\text{C}$  by light scattering at 340 nm using a SPECTRA MAX 190(Molecular Device) spectrophotometer. The plateau absorbance values were used for calculations.

### **2.8 Cellular thermal shift assay (CETSA)**

The ability of Ferulin C to interact with and stabilize microtubule protein in intact cells, was analyzed as described by Molina et al [16]. Briefly, cells cultured in 100 x 20 mm tissue culture dishes at 90% confluence were treated with media containing DMSO or Ferulin C (20  $\mu\text{M}$ ) for 6 hours. After that cells were detached with trypsin and resuspended in PBS. The cell suspension was heated for 3 minutes to 49, 51, and  $53^{\circ}\text{C}$ . Subsequently, cells were lysed using liquid nitrogen and two repeated cycles of freeze-thaw. Precipitated proteins were separated from the soluble fraction by centrifugation at 17,000g for 20 minutes. Soluble proteins, collected in the supernatant, were kept at  $-80^{\circ}\text{C}$  until Western blot analysis.

### **2.9 Autophagy, apoptosis and cell cycle assays**

For the autophagy assay, MCF-7 and MDA-MB-231 cells were transfected with GFP/mRFP-LC3 then treated with 20  $\mu\text{M}$  Ferulin C for 24h and the autophagy ratios were observed under a fluorescence microscope. For apoptosis assay, MCF-7 and MDA-MB-231 cells were treated with 20  $\mu\text{M}$  Ferulin C and apoptosis ratios were determined by flow cytometry analysis of Annexin-V/PI double staining. TUNEL staining was also used to detect cell apoptosis [17]. Cells were treated with DMSO or Ferulin C and then formalin-fixed. TUNEL staining was performed using a One-Step TUNEL Apoptosis Assay Kit (Beyotime, C1086) according to the manufacturer's instructions, with apoptotic cells exhibiting green nuclear fluorescence. For cell cycle detection, MCF-7 and MDA-MB-231 cells were treated with 20  $\mu\text{M}$  Ferulin C for 24h and then ethyl alcohol-fixed at  $4^{\circ}\text{C}$  for 24h. Then the cell cycle distribution were determined by flow cytometry analysis of PI staining.

### **2.10 Cell-migration assays.**

Wound healing assay and Transwell assay were performed to determine the Cell-migration

ability [18, 19]. For Wound healing assay, Cells were seeded in 6-well plate and after cells reached confluency, wounds were created by the manual scraping of the cell monolayer with a pipette tip. The wells were then washed with PBS and added DMSO control or Ferulin C. After 24 h incubation, replenished with PBS and photographed using a phase-contrast microscope. For Transwell assay, Cells were seeded into the upper chamber of a Transwell insert (6.5 mm diameter, 8 mm pores; Corning, New York, USA) at a density of  $1.5 \times 10^4$  cells per well, DMEM (500 mL) with 10% FBS was added to the lower chamber, and the 24-well plate was incubated for 24 h. The cells were treated with DMSO control or Ferulin C for 24 h. The non-migrated cells were scraped off the upper surface of the membrane with a cotton swab and the migrated cells were dyed with crystal violet. After washed by PBS photographed using a phase-contrast microscope.

### **2.11 Transfection assays**

Cells were transfected with p21<sup>Waf1/Cip1</sup> (6456, CST), PAK1,  $\beta$ -Tubulin and negative control (6568, CST) siRNAs/plasmids at 100 nM final concentration using Lipofectamine RNAiMAX/Lip3000 reagent (Invitrogen) according to the manufacturer's instructions. The transfected cells were used for subsequent experiments 48 h later.

### **2.12 RNA-sequencing (RNA-seq) analysis**

Total RNA of Ferulin C-treated group and control group were extracted using TRIzol Reagent (Invitrogen, USA), and quantified by NanoDrop (Thermo Fisher Scientific, USA). RNA-seq analysis was performed on HiSeq X Ten instrument (Illumina, huada gene, Wuhan, China). The obtained data underwent quality trimming to remove low-quality bases using Cutadapt version 1.9.1, followed by aligned to the mouse genome (*Mus musculus*. GRCm38) downloaded from the NCBI database. Differential mRNA expression analysis was carried out using the DESeq2, version 1.6.3 [20]. The adjusted p-value of  $<0.05$  was set to detect differentially expressed genes with at least two-fold change of expression.

### **2.13 Immunofluorescence analysis**

The MCF-7 and MDA-MB-231 were sequentially incubated, starting with  $\alpha$ -tubulin antibody (1:200),  $\beta$ -tubulin(1:200), p-AKT(1:200), PAK1(1:200) and E-cadherin antibody (1:200) diluted in PBS containing 1% BSA incubated overnight at 4°C, followed by addition of fluorescent-labeled secondary antibodies (TRITC, ab6718; Alexa Fluor 488, ab150077) for 1 h at room

temperature.

#### **2.14 Western blot**

Adherent and floating cells were collected after treatment with Ferulin C for indicated times. Cells were lysed in a lysis buffer consisting of Hepes 50 mM pH 7.4, Triton-X-100 1%, sodium orthovanada 2 mM, sodium fluoride 100 mM, edetic acid 1 mM, PMSF 1 mM, aprotinin (Sigma, MO, USA) 10 mg/L and leupeptin (Sigma) 10 mg/L at 4°C for 1 h. After 12,000 rpm centrifugation for 15 min, the protein content of supernatant was determined by the Bio-Rad DC protein assay (Bio-Rad Laboratories, Hercules, CA, USA). Equal amounts of the total protein were separated by 10-15% SDS-PAGE and transferred to PVDF membranes, and the membranes were soaked in blocking buffer (5% skimmed milk or BSA). Proteins were detected using primary antibodies, followed by HRP-conjugated secondary antibody and visualized by using ECL as the HRP substrate. Quantity One 4.4 was used to quantify.

#### **2.15 Xenograft breast cancer model**

The animal experiments were conducted under the guidelines of Shenzhen University Committee for Use and Care of Animals. 60 female BALB/c mice (6-8 weeks, 20-22 g), which were purchased from Liaoning chang sheng biotechnology co., Ltd, and housed in groups of five mice per cage. Animals were acclimatized for one week prior to the experiment under controlled temperature ( $25\pm 2^{\circ}\text{C}$ ) and a reverse 12 h light-dark cycle. Animals had *ad libitum* access to water and food throughout the experiment. MCF-7 cells ( $5 \times 10^6$  cells/mouse) were injected subcutaneously to mice. When the tumors reached about 100 mm<sup>3</sup> in volume, the optimized mice were randomly assigned into four groups (n = 10), including a control group and three Ferulin C-treated groups. Three Ferulin C-treated groups were challenged with different doses of Ferulin C once a day by intragastric administration for 16 days (low dose, 25 mg/kg; median dose, 50 mg/kg; high dose, 100 mg/kg), whereas the control group was treated with vehicle. Animals were weighed three times per week during the treatment, and tumor size was measured three times per week by electronic calipers during the treatment period. All mice were sacrificed, and the tumor tissues were harvested, weighed, and photographed. Then, the tumor tissues were frozen in liquid nitrogen or fixed in formalin immediately for further investigation.

#### **2.16 Statistical analysis**

The results were expressed as means  $\pm$  SEM. Differences between two groups were processed

by Student's unpaired t test by GraphPad Prism 7.00 software. Multi-groups comparisons of the means were carried out by one-way analysis of variance (ANOVA) test with post hoc contrasts by Student–Newman–Keuls test. All the presented data was confirmed by at least three independent experiments.  $P < 0.05$  was considered statistically significant.

### 3 Results

#### 3.1 The total synthesis of Ferulin C

To afford enough amount of Ferulin C, we designed and completed the total synthesis of Ferulin C successfully for the first time. The preparation of Ferulin C was carried out by using commercially available **1** (resorcinol) (**Figure 1**). The intermediate **2** was prepared by Friedel–Crafts reaction of resorcinol with glacial acetic acid, and intermediate **2** reacted with dimethyl sulfate to give intermediate **3**. Treatment of intermediate **3** with diethyl carbonate afforded intermediate **4**. Intermediate **6** was yielded by bromide reaction of farnesol with phosphorus tribromide. The reaction of intermediate **4** with intermediate **6** yielded compound **7**. Ferulin C (**Figure 2A**) was prepared by oxidative cyclization reaction of compound **7**.

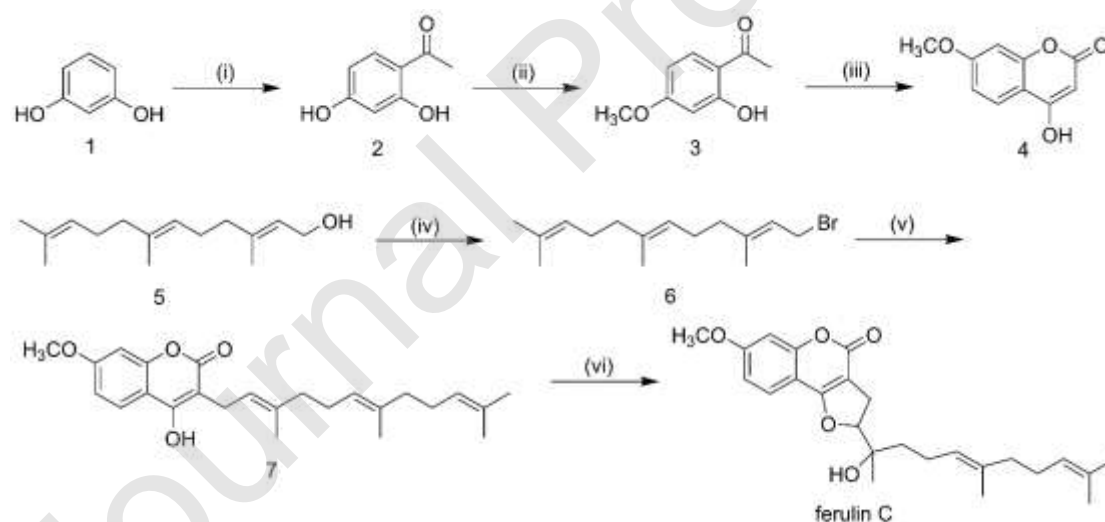


**Figure 1** General synthesis of Ferulin C. Reagents and conditions: (i)  $\text{ZnCl}_2$ , AcOH, reflux; (ii)  $\text{SO}_2(\text{OCH}_3)_2$ ,  $\text{K}_2\text{CO}_3$ , acetone, reflux; (iii) NaH,  $\text{CO}(\text{OEt})_2$ , toluene, reflux; (iv)  $\text{PBr}_3$ ,  $\text{CH}_2\text{Cl}_2$ ; (v) 4, NaI,  $\text{Et}_3\text{N}$ ; (vi) MCPBA, NaOAc,  $\text{CH}_2\text{Cl}_2$ .

#### 3.2 Ferulin C is a potent microtubule-destabilizing agent with antiproliferatory activity

In antiproliferative assays, Ferulin C exhibited potent antiproliferative activity in a dose- and time-dependent manner in MCF-7 ( $\text{IC}_{50}=19.8 \mu\text{M}$ , 24 h) and MDA-MB-231 ( $\text{IC}_{50}=15.6 \mu\text{M}$ , 24

h) cells (**Figure 2B**), and the colony formation assay further confirm the antiproliferative effect of Ferulin C ( $P < 0.0001$ ) (**Figure 2C**). To investigate potential targets of Ferulin C, a reverse molecular docking method was adopted through Discovery Studio 3.5 with the scPDB database including 117,423 pharmacophores [21]. The results revealed that  $\beta$ -tubulin (PDB code 4o2a) was the most likely target with a higher score and biological functions closely related to cancer (**Table S1**). In order to further confirm the hypothesis, molecular docking and MD were performed to elucidate the potential interactions. The RMSD of C $\alpha$  atoms for the residues in 5 Å around ligand is stable within 70 ns (**Figure 2D**). Subsequently, the binding free energy of the system was calculated by MM/GBSA method, revealing that Ferulin C bears favorable energy with  $\Delta H_{\text{bind}}$  value of -49.00 kcal/mol (**Figure 2E**). Additionally, the MM/GBSA decomposition analysis revealed that residues Leu246, Ala248, Leu253, Asn256, Met257, Thr302, Val303, Ala304, Val339, and Ala342 play a vital role in the binding of Ferulin C -  $\alpha/\beta$ -tubulin (**Figure 2F**). As presented in **Figure 2G**, **Figure S1**, **S2**, Ferulin C binds to the same site as colchicine at  $\beta$ -tubulin. The furan coumarin core of Ferulin C is buried in the colchicine site at the intradimer interface, forming mainly hydrophobic contacts with  $\beta$ -tubulin. The 7-position methoxyl forms a hydrogen bond with the side chain of Lys340. Another key hydrogen bond is also observed between the lactone carbonyl group of coumarin and Thy302 of  $\beta$ -tubulin. Besides, the furan oxygen atom initiates a key hydrogen bond interaction with the side chain of Asn256. Furthermore, the side chain hydroxy of Ferulin C interacts with Leu253 and Asn256 to build two additional hydrogen contacts. The above interactions suggest that Ferulin C is a potential  $\beta$ -tubulin inhibitor, binding to the colchicine binding site. Next, we conducted the Tubulin Polymerization Assay to confirm the inhibitory activity of Ferulin C against tubulin polymerization. The results revealed that Ferulin C could significantly suppress the Tubulin Polymerization with  $IC_{50}$  of 9.2  $\mu\text{M}$  (**Figure 2H**) and Colchicine was used as the reference compound ( $IC_{50} = 1.8 \mu\text{M}$ ) (**Figure S3**). In addition, the CESTA assay demonstrated that Ferulin C could stabilize  $\beta$ -Tubulin protein in intact cells, but the effect was not significant (**Figure S4**). Collectively, these findings substantiated that Ferulin C is a novel potent tubulin polymerization inhibitor.

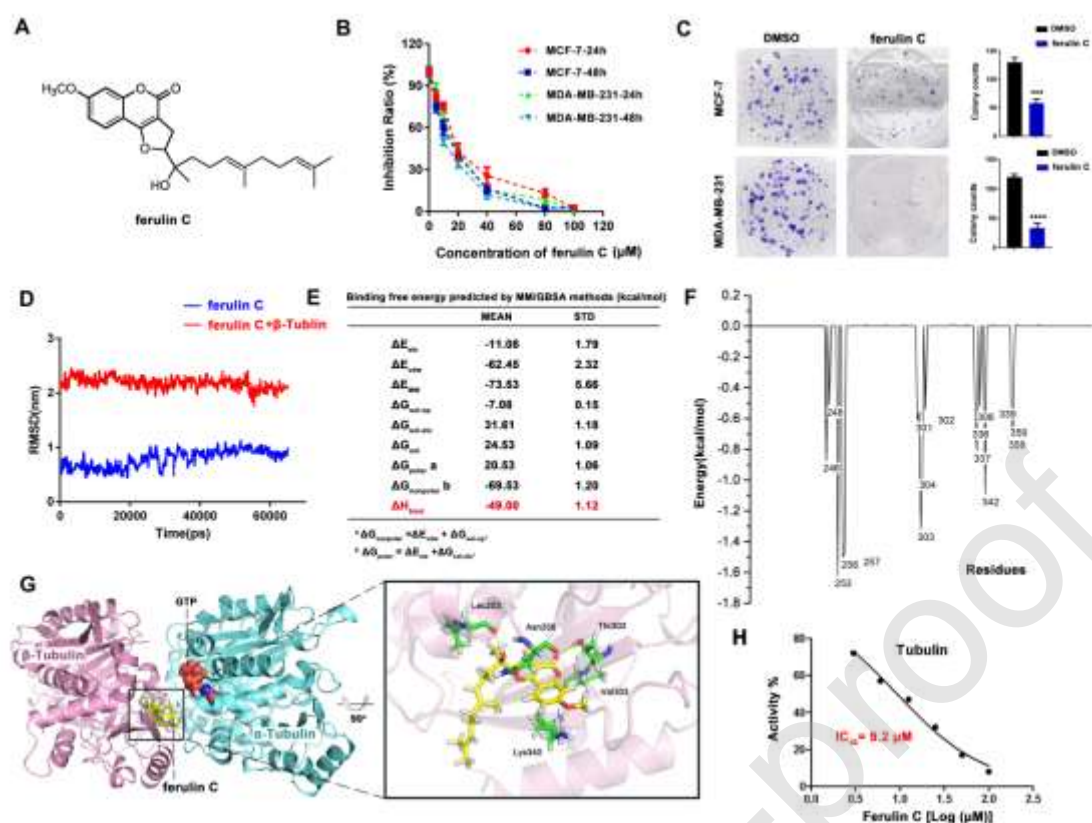


**Figure 2.** Ferulin C is a potent tubulin polymerization inhibitor. (A) The structure of Ferulin C; (B) MTT assays were performed to measure the antiproliferative potency of Ferulin C against MCF-7 and MDA-MB-231 cells. (C) Colony formation assay of MCF-7 and MDA-MB-231 cells treated with 20  $\mu\text{M}$  Ferulin C for two weeks. Representative images (Left) and quantification of colonies (Right) were shown (\*\*,  $P < 0.001$ ;\*\*\*\*,  $P < 0.0001$ ). (D) The RMSD plot of MD of Ferulin C and  $\alpha/\beta$ -tubulin complex; (E) Binding free energy predicted by MM/GBSA methods; (F) The binding energies on a per-residue basis were calculated based on the MM/GBSA decomposition analysis; (G) Molecule docking of Ferulin C and  $\alpha/\beta$ -tubulin and a detailed show of interaction between Ferulin C and  $\alpha/\beta$ -tubulin. Molecular dynamics of Ferulin C and  $\alpha/\beta$ -tubulin complex. (H) Effect of Ferulin C on tubulin polymerization.

### 3.3 Effect of Ferulin C on microtubule assembly

In immunofluorescence on microtubule assembly, Ferulin C induced significant microtubule dynamic instability in both MCF-7 and MDA-MB-231 cells. Ferulin C disturbed the microtubule integrity and structure mainly through suppressing the assembly of  $\beta$ -tubulin and inducing its abnormal accumulation (**Figure 3C, D**), while less effect on the structure of  $\alpha$ -tubulin (**Figure 3A, B**), which is consistent with the prediction that Ferulin C binds to the colchicine site located

the intradimer interface of  $\alpha$ - and  $\beta$ -tubulin, resulting in microtubule depolymerization. These findings further confirmed that Ferulin C is a potent tubulin polymerization inhibitor in MCF-7 and MDA-MB-231 cells.

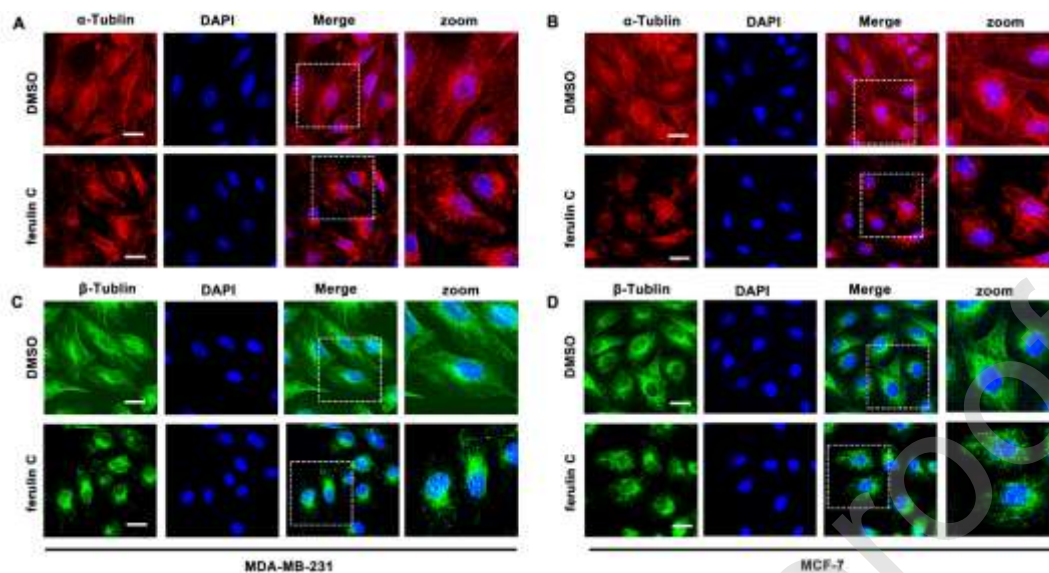


**Figure 3.** Effects of Ferulin C on microtubule integrity and structure. Immunofluorescence confocal microscopy images of MCF-7 and MDA-MB-231 cells treated with DMSO (control) or 20 $\mu$ M Ferulin C. The nuclei and microtubules have been labeled with DAPI (blue),  $\alpha$ -tubulin antibody (red) and  $\beta$ -tubulin (green), respectively. Scale bar=10  $\mu$ m.

### 3.4 Ferulin C induced G1/S cell cycle arrest via p21<sup>Cip1/Waf1</sup> - CDK2 signaling pathway

Microtubules are essential in the mitosis process, and microtubule inhibitors could disturb the progress of the cell cycle [7]. In cell cycle examination, Ferulin C induced a concentration-dependent increase in G1/S phase arrest (**Figure 4A, B**). To elucidate the mechanism, we checked some key cell cycle regulators (**Figure 4C**), revealing that Ferulin C could up-regulate p21<sup>Cip1/Waf1</sup>, inhibited the phosphorylation of CDK2 at Thr160 and dramatically down-regulated the expression and phosphorylation of Cyclin E1 in both MCF-7 and MDA-MB-231 cells. Furthermore, we knocked down p21<sup>Cip1/Waf1</sup> by specific siRNA, found that CDK2/Cyclin E signaling was activated, and Ferulin C had less effect on them after p21<sup>Cip1/Waf1</sup> silencing (**Figure 4D**). Taken together, Ferulin C induced G1/S cell cycle arrest via p21<sup>Cip1/Waf1</sup> - CDK2 signaling pathway.

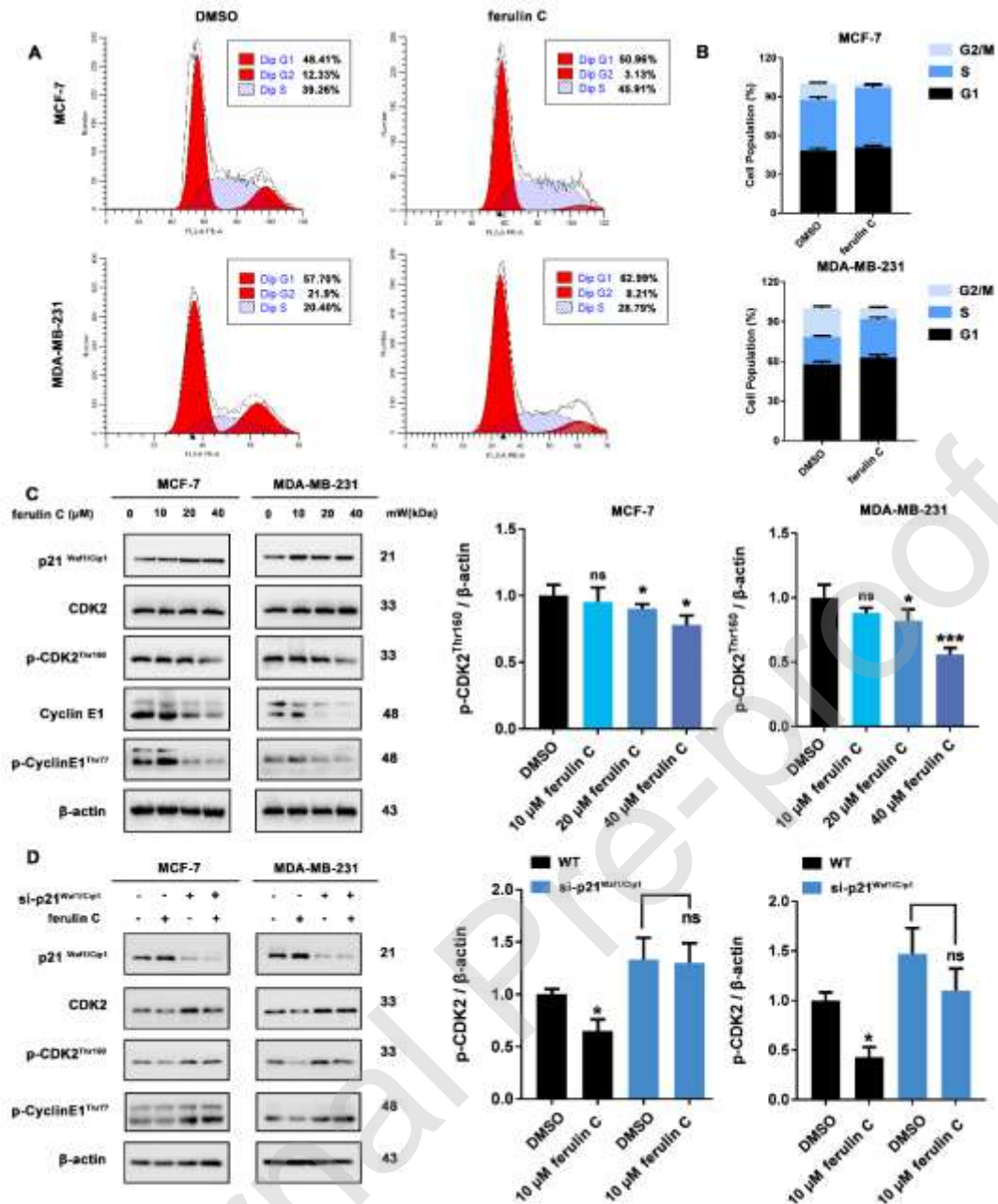


**Figure 4.** Ferulin C causes G1/S cell cycle arrest, up-regulation of p21<sup>Cip1/Waf1</sup> and inhibition of CDK2/Cyclin E1 in breast cancer cells. (A, B) MCF-7 and MDA-MB-231 cells treated with 20  $\mu$ M Ferulin C or DMSO (control) for 24 hours and subjected to cell cycle analysis following treatment with propidium iodide. (C) Western blot analysis of p21<sup>Cip1/Waf1</sup>, CDK2, p-CDK2<sup>Thr160</sup>, Cyclin E1 and p-Cyclin E1<sup>Thr77</sup> in MCF-7 and MDA-MB-231 cells treated with 10, 20, 40  $\mu$ M of Ferulin C for 24 h. The relative p-CDK2<sup>Thr160</sup> expression level was quantified by normalization to  $\beta$ -actin. ns, not significance; \* $p$ <0.05 and \*\*\* $p$ <0.001, compared to DMSO treated Control. (D) MCF-7 and MDA-MB-231 cells transfected with si-NC or si-p21<sup>Cip1/Waf1</sup> were treated with 20  $\mu$ M Ferulin C for 24 h, western blot analysis of p21<sup>Cip1/Waf1</sup>, CDK2, p-CDK2<sup>Thr160</sup> and p-Cyclin E1<sup>Thr77</sup>.

The relative p-CDK2<sup>Thr160</sup> expression level was quantified by normalization to  $\beta$ -actin. ns, not significance; \* $p < 0.05$ , compared to DMSO treated Control.

### 3.5 Ferulin C induced classical apoptosis in MCF-7 and MDA-MB-231 cells

p21<sup>Cip1/Waf1</sup> acts not only as an inhibitor of cell cycle progression but also as an important regulator of apoptosis. Firstly, TUNEL assay was performed to examine whether Ferulin C could induce apoptosis with obvious FITC fluorescence aggregated in the nucleus (**Figure 5A**). Next, Annexin-V/PI staining analysis revealed that a significant increase in early and late apoptotic cells in the presence of Ferulin C was observed, indicating that Ferulin C could elicit obvious apoptosis (**Figure 5B**). Additionally, Ferulin C also substantially elevated the expression of 14-3-3 and Bax, reduced the expression of Bcl-2, accompanied with the cleavage of caspase3, caspase7, caspase9 and PARP, which suggested the activation of the classical mitochondria apoptotic pathway (**Figure 5C**). Notably, Ferulin C could also up-regulate Fas, FADD and caspase8 to activate death receptor apoptosis pathway (**Figure 5D**). Therefore, Ferulin C is capable of inducing classical apoptosis in breast cancer cells.

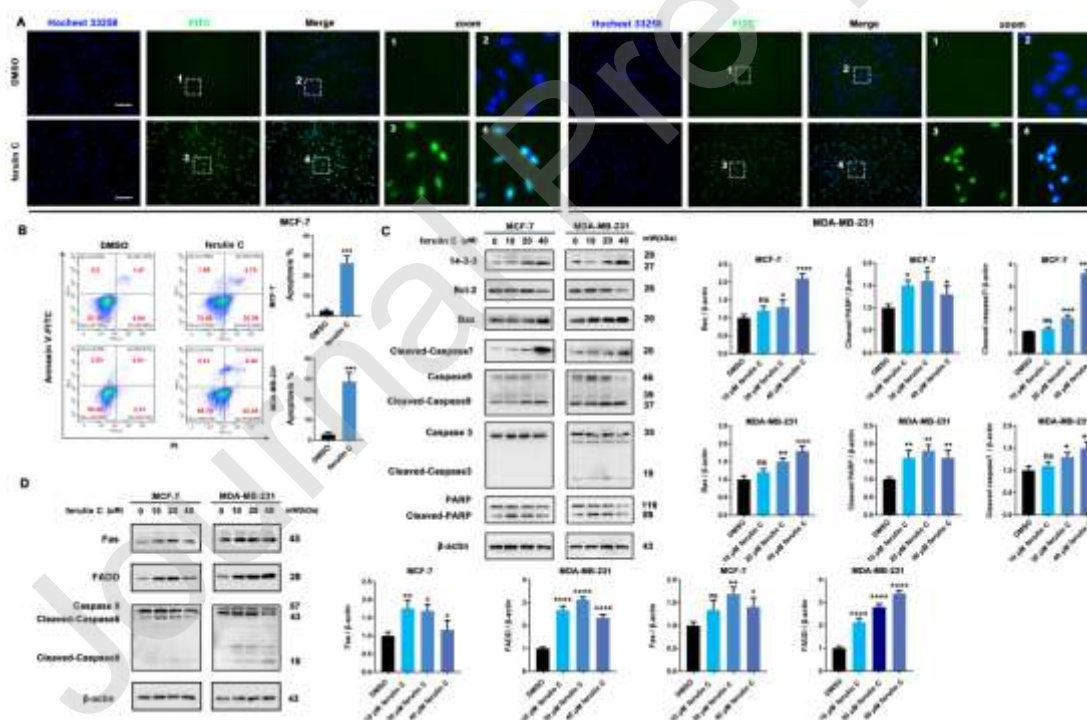


**Figure 5.** Ferulin C induced apoptosis in breast cancer cells. (A) MCF-7 and MDA-MB-231 cells were treated with 20  $\mu$ M Ferulin C for 24h, apoptosis were evaluated by TUNEL assay. Scale bar = 80  $\mu$ m. (B) MCF-7 and MDA-MB-231 cells were treated with 20  $\mu$ M Ferulin C for 24h, apoptosis ratios were determined by flow cytometry analysis of Annexin-V/PI double staining.

(C) Western blot analysis of 14-3-3, Bax, Bcl-2, Caspase8, Caspase3, Caspase9, Caspase7, and PARP in MCF-7 and MDA-MB-231 cells treated with 10, 20, 40  $\mu$ M of Ferulin C for 24 h. Relative Bax, Cleaved PARP and Cleaved caspase7 expression levels were quantified by normalization to  $\beta$ -actin. ns, not significance; \* $p$ <0.05, \*\* $p$ <0.01, \*\*\* $p$ <0.001 and \*\*\*\* $p$ <0.0001, compared to DMSO treated Control. (D) Western blot analysis of Fas, FADD and Caspase8 in MCF-7 and MDA-MB-231 cells treated with 10, 20, 40  $\mu$ M of Ferulin C for 24 h. Relative Fas and FADD expression levels were quantified by normalization to  $\beta$ -actin. ns, not significance; \* $p$ <0.05, \*\* $p$ <0.01 and \*\*\*\* $p$ <0.0001, compared to DMSO treated Control.

### 3.6 Ferulin C suppressed metastasis via Ras-Raf-MEK-ERK signaling

Metastasis is closely associated with poor clinical outcomes due to the limited treatment options available. In wound healing and Transwell assay, Ferulin C obviously inhibited the migration of MCF-7 and MDA-MB-231 cells (**Figure 6A-D**). Furthermore, the expression of E-cadherin was investigated after Ferulin C treatment. As shown in **Figure 6E**, Ferulin C up-regulated E-cadherin conspicuously. To further investigate the potential mechanism of Ferulin C-induced metastasis inhibition, we checked key signaling involved in cancer migration and metastasis. The results indicated that Ferulin C could inhibit Ras-Raf-MEK-ERK signaling with the down-regulation of phosphorylation of c-Raf, MEK1/2 and ERK1/2 (**Figure 6F, G**). Moreover, Ferulin C also inhibited the expression of MMP-2 and up-regulated E-cadherin considered to be associated with cell migration and invasion (**Figure 6F, G**). Collectively, these results demonstrated that Ferulin C suppressed metastasis via Ras-Raf-MEK-ERK signaling in MCF-7 and MDA-MB-231 cells.

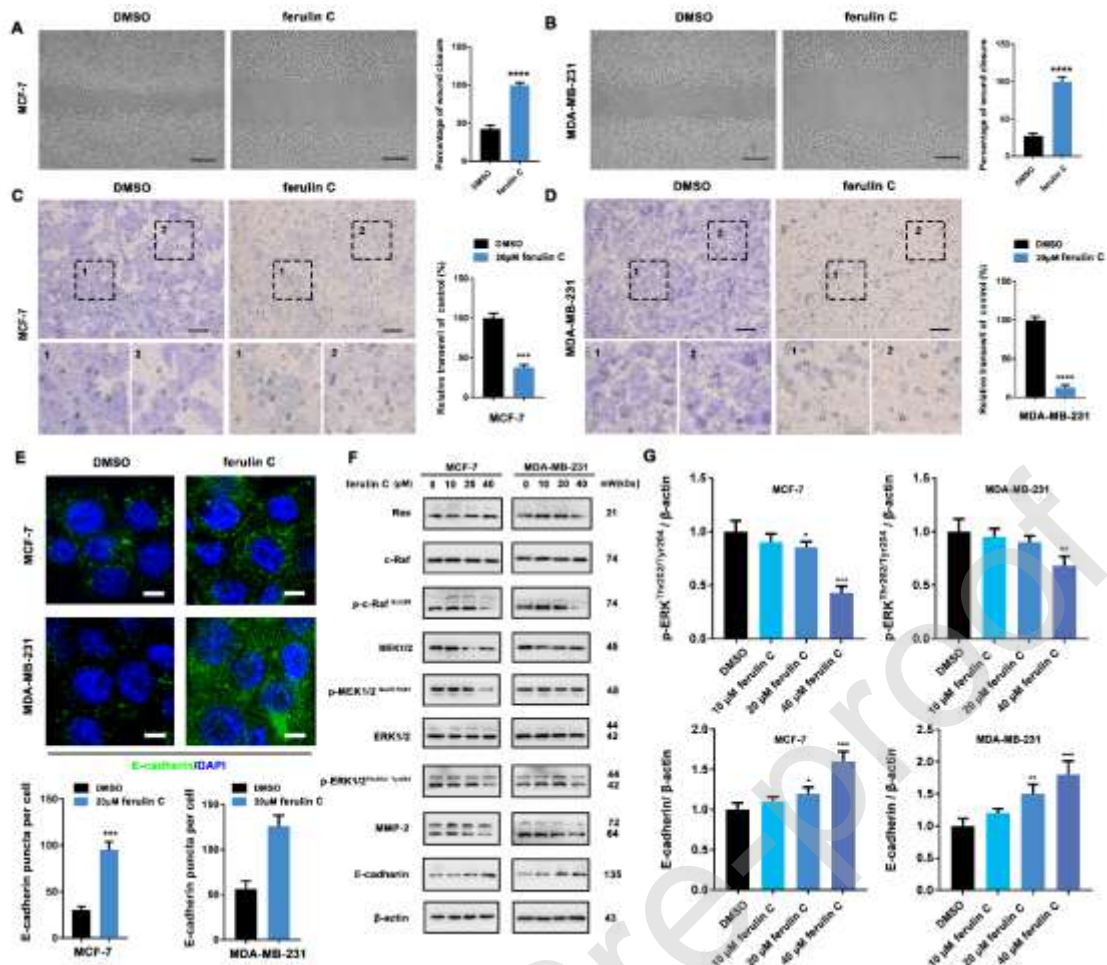


**Figure 6.** Ferulin C suppressed metastasis via ERK1/2 inhibition in breast cancer cells. (A, B) Wound healing assay of MCF-7 and MDA-MB-231 cells treated with 20  $\mu\text{M}$  of Ferulin C for 24 h.  $***p < 0.001$ ,  $****p < 0.0001$ . Scale bar = 200  $\mu\text{m}$ . (C, D) Transwell assay of MCF-7 and MDA-MB-231 cells treated with 20  $\mu\text{M}$  of Ferulin C for 24 h. Scale bar = 40  $\mu\text{m}$ . (E) Representative immunofluorescence images of E-cadherin in MCF-7 and MDA-MB-231 cells treated with 20  $\mu\text{M}$  Ferulin C for 24 h. The number of E-cadherin puncta per cell was quantified by Image J software,  $**p < 0.01$  and  $***p < 0.001$ . Scale bar = 5  $\mu\text{m}$ . (F, G) Western blot analysis of Ras, c-Raf, p-c-Raf<sup>Ser259</sup>, MEK1/2, p-MEK1/2<sup>Ser217/221</sup>, ERK1/2, p-ERK1/2<sup>Thr202/Tyr204</sup>, MMP-2 and E-cadherin in MCF-7 and MDA-MB-231 cells treated with 10, 20, 40  $\mu\text{M}$  of Ferulin C for 24 h. Relative p-ERK1/2<sup>Thr202/Tyr204</sup> and E-cadherin expression levels were quantified by normalization to  $\beta$ -actin.  $*p < 0.05$ ,  $**p < 0.01$  and  $***p < 0.001$ , compared to DMSO treated Control.

### 3.7 Ferulin C stimulated autophagy via AKT/mTOR signaling

ERK1/2 signaling has a close relationship with AKT signaling, numerous studies have revealed

that ERK1/2 signaling inhibition would activate AKT signaling [22, 23], So we examined the effect of Ferulin C on AKT signaling. As shown in **Figure 7A**, Ferulin C exhibited significant AKT inhibition activity by decreasing the expression and nuclear localization of p-AKT<sup>Ser473</sup>. In addition, Ferulin C inhibited the expression and phosphorylation of AKT and its downstream member mTOR which is not only a regulator of cell proliferation but also a key regulator of autophagy. Autophagy plays an important role in tumor metastasis and survival. Increasing studies have shown that activation of autophagy contributes to the treatment of breast cancer [24]. We found Ferulin C could activate mTOR downstream member ULK1 considered to be the initiator of autophagy (**Figure 7B**). Obvious aggregation of LC3 puncta was observed following Ferulin C treatment, and Ferulin C increased the ratio of LC3 fluorescence, indicating induction of autophagy (**Figure 7C**). Besides, Ferulin C resulted in the elevation of Beclin 1, Ambra1, LC3-II in a dose-dependent manner, as well as degradation of SQSTM1/p62. (**Figure 7D, E**). These results indicated that Ferulin C functioned as an autophagy inducer in MCF-7 and MDA-MB-231 cells.

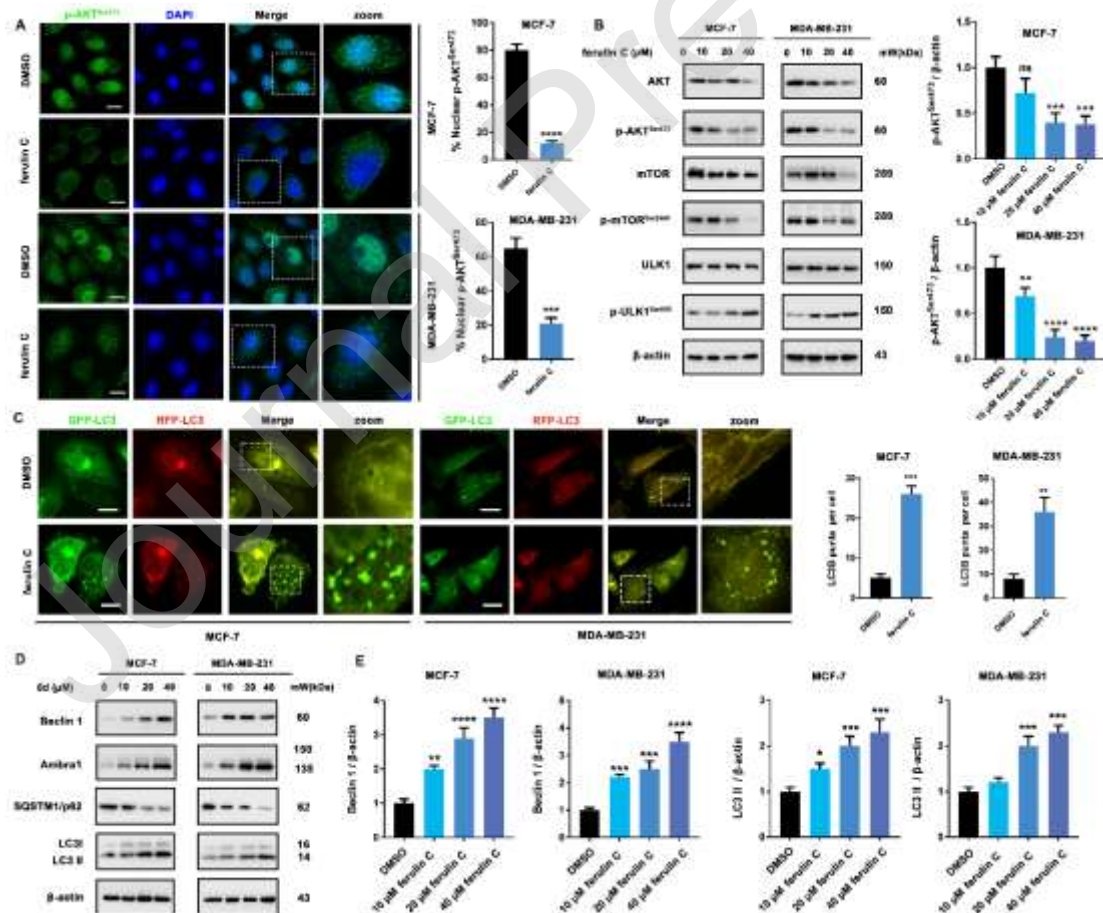


**Figure 7.** Ferulin C induced autophagy in MCF-7 and MDA-MB-231 cells via AKT-mTOR pathway. (A) Representative immunofluorescence images of p-AKT<sup>Ser473</sup> in MCF-7 and MDA-MB-231 cells treated with 20  $\mu$ M Ferulin C for 24 h. The number of E-cadherin puncta per cell was quantified by Image J software, \*\*\* $p$ <0.001 and \*\*\*\* $p$ <0.0001. Scale bar = 5  $\mu$ m. (B) Western blot analysis of AKT, p-AKT<sup>Ser473</sup>, mTOR, p-mTOR<sup>Ser2448</sup>, ULK1 and p-ULK1<sup>Ser555</sup> in MCF-7 and MDA-MB-231 cells treated with 10, 20, 40  $\mu$ M of Ferulin C for 24 h. (C) Representative immunofluorescence images of LC3 puncta in MCF-7 and MDA-MB-231 cells transiently expressing GFP-mRFP-LC3 plasmid followed by treatment of Ferulin C for 24 h. The number of LC3 puncta per cell was quantified by Image J software, \*\* $p$ <0.01, \*\*\* $p$ <0.001. Scale bar = 10  $\mu$ m. (D) Western blot analysis of Beclin 1, Ambra1, SQSTM/p62 and LC3 in MCF-7 and MDA-MB-231 cells treated with 10, 20, 40  $\mu$ M of Ferulin C for 24 h. (E) The relative Beclin1 and LC3-II expression levels were quantified by normalization to  $\beta$ -actin. ns, not significance; \* $p$ <0.05, \*\* $p$ <0.01, \*\*\* $p$ <0.001 and \*\*\*\* $p$ <0.0001.

### **3.8 Ferulin C induced autophagy associated cell death to inhibit proliferation and metastasis**

Autophagy was closely associated with proliferation and metastasis in breast cancer [25]. We employed autophagy inhibitors 3-MA and Bafilomycin A1 to assess the effect of autophagy inhibition on tumor proliferation and metastasis. 3-MA and Bafilomycin A1 treatment decreased the anti-proliferation activity of Ferulin C, and 3-MA increased the migration capabilities of MCF7 cells (**Figure 8A, B**). While in MDA-MB-231 cells, 3-MA and Bafilomycin A1 affect little on the cell viability after Ferulin C treatment, but 3-MA still could promote the ability of cell migration (**Figure 8C, D**). Additionally, we found 3-MA could increase the population of living cells in MCF7 cells while affected less in MDA-MB-231 cells (**Figure 8E, F**). These results indicated autophagy induced by Ferulin C contributed to inhibiting breast cancer cell proliferation and metastasis.

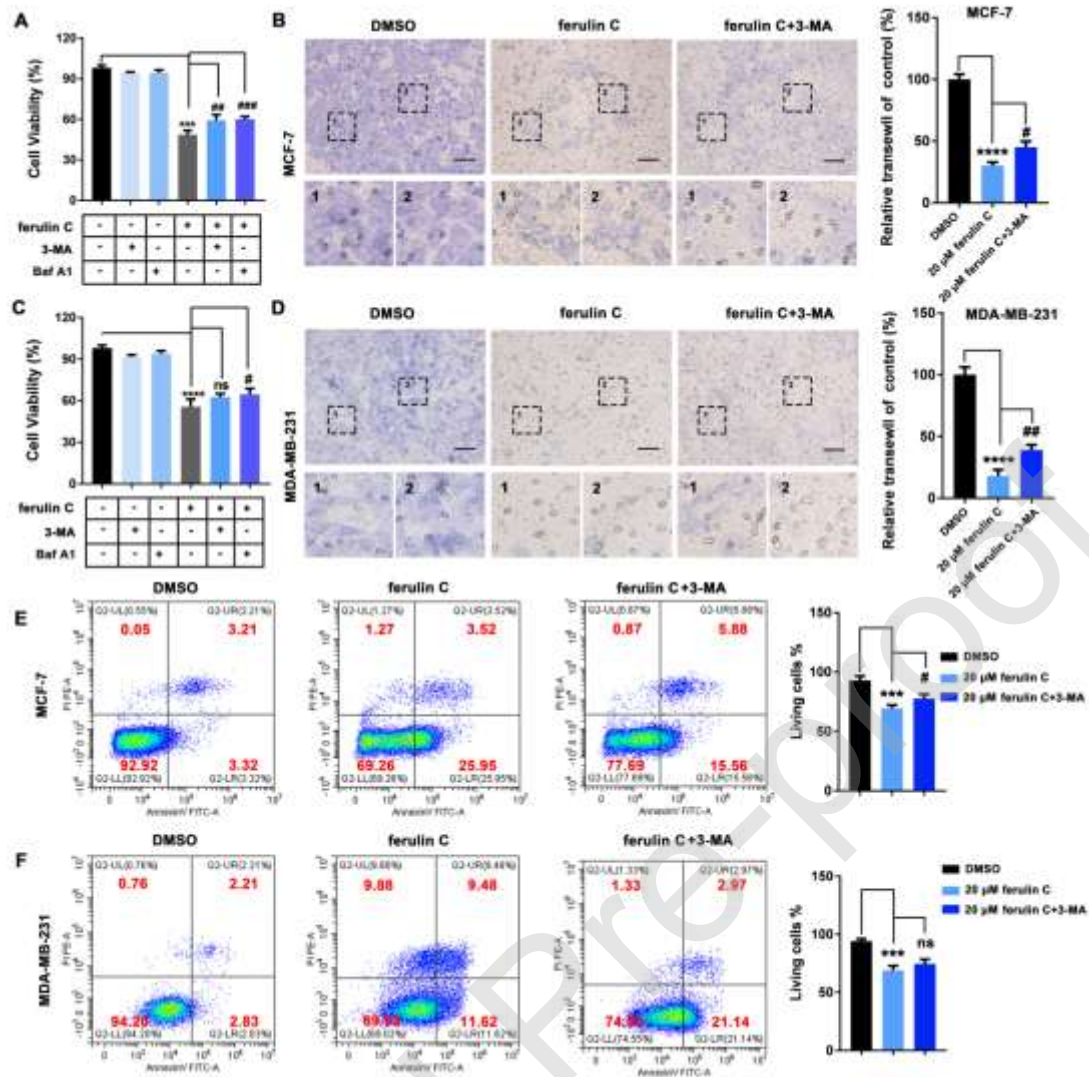


**Figure 8.** Ferulin C induced autophagy-associated cell death to inhibit proliferation and metastasis in breast cancer cells.(A, C) MTT assay to determine the effect of 3-MA and Bafilomycin A1 on cell viability after treated with 20  $\mu$ M Ferulin C for 24 h in MCF7(A) and MDA-MB-231 cells(C). (B, D)Transwell assay of MCF-7(B) and MDA-MB-231 cells. (D) treated with 20  $\mu$ M of Ferulin C with or without 3-MA for 24 h. Scale bar = 40  $\mu$ m. (E, F) MCF-7 and MDA-MB-231 cells were treated with 20  $\mu$ M Ferulin C with or without 3-MA for 24h, apoptosis ratios were determined by flow cytometry analysis of Annexin-V/PI double staining. ns, not significance; \* $p$ <0.05, \*\* $p$ <0.01, \*\*\* $p$ <0.001 and \*\*\*\* $p$ <0.0001.\*,compared with DMSO control; #, compared with 20  $\mu$ M Ferulin C treatment.

### 3.9 Identification of novel regulatory protein PAK1 in Ferulin C-regulated microtubule depolymerization to breast cancer therapy

Next, we constructed the protein-protein interactions (PPI) network of  $\alpha/\beta$ -tubulin by the predicted and experimentally determined protein-protein interactions (PrePPI) [26], in which 54 hub proteins were identified to potentially interact with  $\alpha/\beta$ -tubulin (**Figure 9A**). These related proteins were annotated by Gene Ontology (GO) [27] (**Figure 9B**), presenting that these proteins are closely related to cell apoptosis process, cycle arrest, cell migration, cell proliferation and autophagy. Notably, PAK1 involves multiple regulatory pathways, suggesting that PAK1 maybe play an important role in Ferulin C-regulated microtubule depolymerization to induce breast cancer cells. To confirm the hypothesis, the RNAseq results revealed that Ferulin C treatment induced 1392 probe sets having a  $p < 0.05$  and fold change  $> 2$  (453 genes up-regulated and 939 genes down-regulated) (**Figure 9C**). The top 30 genes were shown in heatmap (**Figure 9D**), *PAK1* was significantly down-regulated, which is consistent with biological information analysis results. Furthermore, these differential genes mainly were involved in cell adhesion, cell proliferation, angiogenesis, cell migration and regulation of ERK1 and ERK2 cascade signaling pathways (**Figure 9E**). Based upon the predicted and RNAseq results, PAK1 was involved in multiple signal processes, including cell cycle, cell migration, cell proliferation, apoptosis and autophagy (**Figure 9F**). According to the Cancer Genome Atlas (TCGA) analysis, elevated expression of PAK1 was associated with poor survival and p21 was associated with better survival in breast cancer patients (**Figure 9G, H**). The results of immunofluorescence and western blot confirmed Ferulin C significantly inhibited the expression of PAK1 in a concentration-dependent manner in MCF-7 and MDA-MB-231 cells (**Figure 10A, B**). In addition, Ferulin C downregulated the expression of PAK1 downstream proteins associated with cell cycle regulation, including CHK2, CDC25A and p-CDC25A<sup>Ser124</sup> (**Figure 10B**). We transfected a constitutively active form of PAK1 (CA-PAK1) and found PAK1 overexpression induced the activation of CDC25A and Ferulin C could not inhibit the phosphorylation of CDC25A (**Figure 10C**). To further clarify the relationship between tubulin inhibition and p21/PAK1, we firstly detected the effect of Ferulin C on tubulin expression and confirmed that Ferulin C did not affect the expression of tubulin (**Figure 10D**). Subsequently, we found that overexpression of  $\beta$ -Tubulin had no significant effect on the expression of PAK1 and p21 in MCF-7 cells. While overexpression of  $\beta$ -Tubulin could upregulate the expression of PAK1 in MDA-MB-231 cells. Of note, whether  $\beta$ -Tubulin is over-expressed or not, Ferulin C

could obviously up-regulated p21 and downregulated PAK1 (**Figure 10E**). This is interesting, but it has further proved that Ferulin C only affects the structure of microtubules and do not affect the expression of tubulin. In summary, Ferulin C induces microtubule instability by disrupting microtubule structure, and subsequently activates p21 and inhibits PAK1.

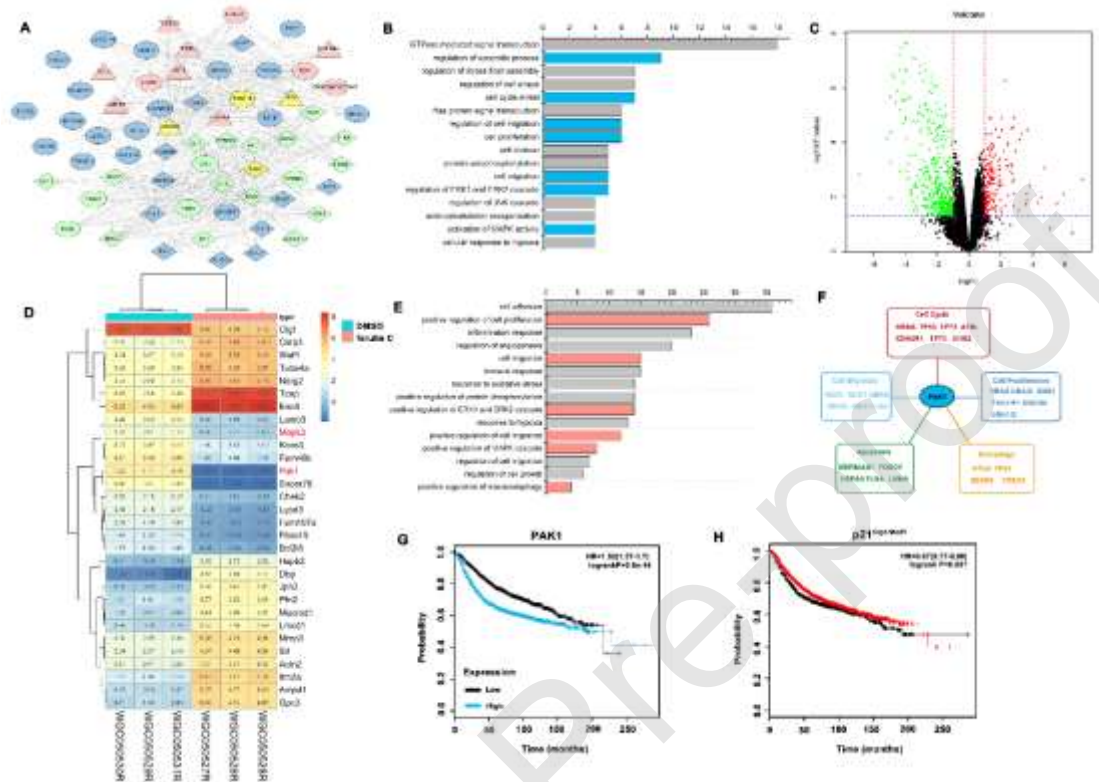


**Figure 9** Identification of novel regulatory protein PAK1 in Ferulin C-regulated microtubule depolymerization. (A) the protein-protein interactions (PPI) network of  $\alpha/\beta$ -tubulin; (B) the Gene Ontology (GO) analysis of hub proteins; (C) Volcano plot of up- and down-regulated genes following Ferulin C treatment in MDA-MB-231 cells; (D) Heatmap of the differential genes with an at least two-fold change in expression in Ferulin C-treatment group compared with DMSO group; (E) the Gene Ontology (GO) analysis of differential genes; (F,H) PAK1 and p21 was involved in multiple signal processes.

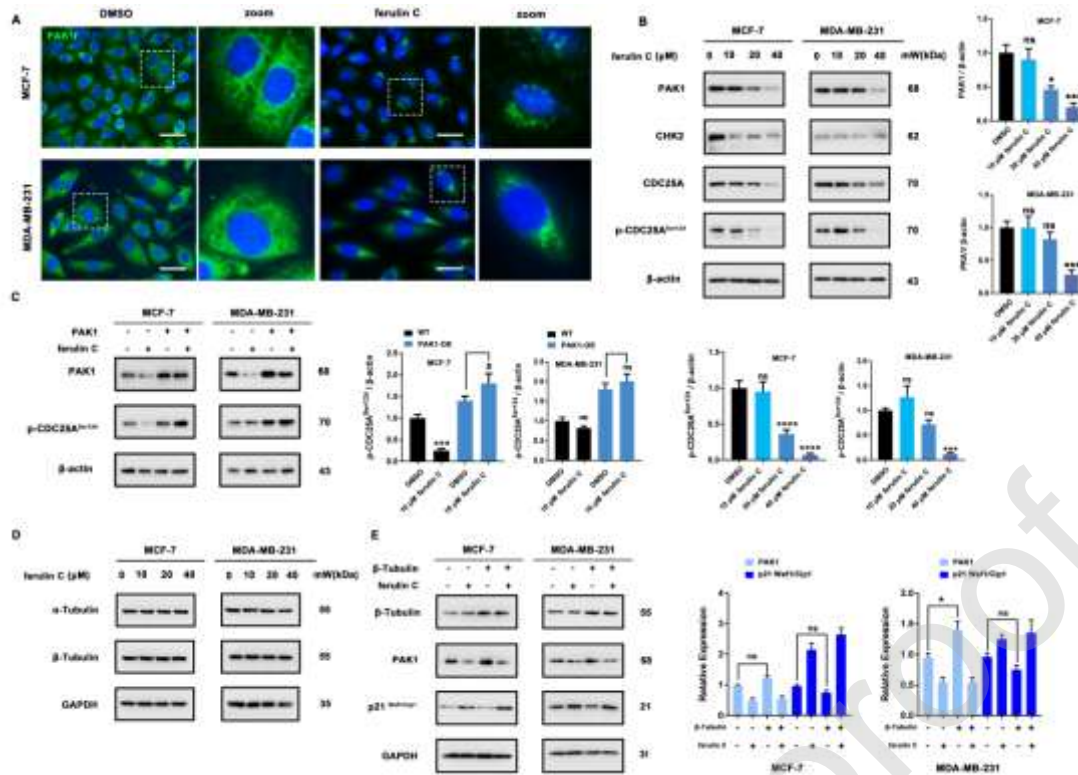


**Figure 10.** Ferulin C inhibited PAK1 to regulate the activation of CDC25A pathway. (A) Representative immunofluorescence images of PAK1 in MCF-7 and MDA-MB-231 cells treated with 20  $\mu$ M Ferulin C for 24 h. Scale bar = 20  $\mu$ m. (B) Western blot analysis of PAK1, CHK2, CDC25A, p-CDC25A<sup>Ser124</sup> in MCF-7 and MDA-MB-231 cells treated with 10, 20, 40  $\mu$ M of Ferulin C for 24 h. The relative PAK1 and p-CDC25A<sup>Ser124</sup> expression levels were quantified by normalization to  $\beta$ -actin. ns, not significance; \* $p$ <0.05, \*\*\* $p$ <0.001. (C) MCF-7 and MDA-MB-231 cells transfected with Vector or CA-PAK1 were treated with 20  $\mu$ M Ferulin C for 24 h, Western blot analysis of PAK1 and p-CDC25A<sup>Ser124</sup>. The relative p-CDC25A<sup>Ser124</sup> expression level was quantified by normalization to  $\beta$ -actin. ns, not significance; \* $p$ <0.05, \*\*\* $p$ <0.001. (D) Western blot analysis of  $\alpha$ -Tubulin,  $\beta$ -Tubulin in MCF-7 and MDA-MB-231 cells treated with 10, 20, 40  $\mu$ M of Ferulin C for 24 h. GAPDH as the loading control. (E) MCF-7 and MDA-MB-231 cells transfected with Vector or CA- $\beta$ -Tubulin were treated with 20  $\mu$ M Ferulin C for 24 h, Western blot analysis of  $\beta$ -Tubulin,  $\alpha$ -Tubulin, PAK1 and p21. The relative PAK1 and p21 expression levels were quantified by normalization to GAPDH. ns, not significance; \* $p$ <0.05.

### 3.10 Ferulin C inhibits the growth of xenograft breast cancer

To evaluate the potency of Ferulin C *in vivo*, we established an MCF-7 cells xenograft model. Based on the results of tumor weight and volume, Ferulin C could significantly inhibit the growth of xenograft MCF-7 cells (**Figure 11A, B**). The body weights of mice were stable, with no obvious distinctions between Ferulin C-treated and control mice (**Figure 11C**). Next, we examined the immunoreactivity of Ki-67 and LC3B in tumor tissues and found Ferulin C inhibited the expression of Ki-67 and promoted the expression of LC3B (**Figure 11D, E**). To further confirm the mechanisms for the therapeutic efficacy of Ferulin C, we carried out western blot to analyze key regulators identified *in vitro*. Ferulin C inhibited the expression of PAK1, p-ERK<sup>Thr202/Tyr204</sup>, p-AKT<sup>Ser473</sup> and up-regulated E-cadherin, Bax, Beclin 1 and LC3II (**Figure 11F**), which is in correlation with *in vitro*. In summary, Ferulin C exhibited good therapeutic potential of breast cancer *in vivo*.



relative PKA1, p-ERK<sup>Thr202/Tyr204</sup>, E-cadherin and LC3II expression level was quantified by normalization to  $\beta$ -actin. ns, not significance; \* $p < 0.05$ , \*\* $p < 0.01$ , \*\*\* $p < 0.001$  and \*\*\*\* $p < 0.0001$ ; (G) The schematic model of Ferulin C-induced cell death pathways, associated with apoptosis, cell cycle arrest, autophagy and metastasis.

#### 4. Discussion

In the present study, we have completed the total synthesis of Ferulin C for the first time. In cell viability assay, Ferulin C displayed potent antiproliferative activity against MCF-7 and MDA-MB-231 cells with concentration-dependent manners (What must be explained is that the inhibitory activity of Ferulin C against MCF-7 cells was incorrect in our previous report [28], which might be resulted from the inaccurate amount of Ferulin C because of the small amount, we make a corresponding correction). Furthermore, Molecular docking and molecular dynamics simulations further elucidated the binding modes and dynamics characteristics of Ferulin C and  $\beta$ -tubulin, the results suggested that Ferulin C is a potent  $\beta$ -tubulin inhibitor binding to the colchicine site. The CETSA assay also confirmed Ferulin C could bind to  $\beta$ -tubulin and tubulin polymerization assay to confirm the inhibitory activity of Ferulin C against Tubulin Polymerization. Microtubule destabilization induced by Ferulin C changed the intracellular environment, activated p21 and inhibited PAK1 activity. Additionally, Ferulin C elicited G1/S cell cycle arrest via  $p21^{Cip1/Waf1}$  - CDK2 signaling pathway and activated  $p21^{Cip1/Waf1}$ -regulated apoptosis pathway by increasing the expression of 14-3-3 and Bax, reduced the expression of Bcl-2 and stimulating the activation of the classical apoptotic proteins. Namely, the activation of p21 promotes cell cycle arrest and apoptosis. Furthermore, Ferulin C suppressed metastasis via ERK1/2 inhibition and induced autophagy in MCF-7 and MDA-MB-231 cells. The inhibition of PAK1 impaired the Raf-MEK1/2-ERK1/2 and CHK2-CDC25A signaling, resulting in inhibiting cell proliferation and metastasis. In addition, the inhibition of AKT-mTOR signaling and autophagy associated cell death stimulated by mTOR further contributed to blocking cell proliferation and metastasis (**Figure 11G**). Ferulin C displayed an acceptable cancer inhibition in an MDA-MB-231 xenograft model *in vivo*. However, Ferulin C bears less tubulin polymerization inhibitory activity compared to Colchicine, Ferulin C shows a novel anti-cancer mechanism in spite of they bear the similar microtubule inhibition function. Colchicine exerts antiproliferative effects through the inhibition of microtubule formation by blocking the cell cycle

at the G2/M phase and triggering apoptosis [29]. Of note, in our study, MDA-MB-231 cells were more sensitive to Ferulin C than MCF-7 cells. This is interesting because the malignancy of MDA-MB-231 cells are higher than MCF-7 cells. We observed that metastasis inhibition activity of Ferulin C on MDA-MB-231 cells was more puissant and autophagy induction effect of Ferulin C was more contribute to its anti-cancer effect. Cells of the same cancer type respond differently to the same drug, which is an annoying and worthwhile question. We believe that with the deepening of the research, there is a subtype of cancer that is more suitable for Ferulin C treatment.

## **5. Conclusion**

In summary, our data defined Ferulin C as a potent, colchicine site binding, microtubule-destabilizing agent with potent anti-proliferation and anti-metastasis activity via PAK1 and p21-mediated signaling in breast cancer cells. Therefore, Ferulin C can be a potential anti-tumor agent for breast cancer treatment.

## **Author Contribution**

J-H W, Z-D H and Jin Zhang designed the research; D-H Y, D-B P, Y-Q Z and J Z performed experiments; D-H Y wrote and edited the manuscript; D-H Y carried out the data analysis.

## **Conflicts of Interest**

The authors declare no conflict of interest.

## **Acknowledgments**

This work was received the supported of Key Projects of the National Science and Technology Major Projects for New Drug Development (2018ZX097350052), The National Key R & D Program of China (2017YFA0503900), National Natural Science Foundation of China (31670360, 81803365 and U1702286) and Post-Doctor Research Project (2018M643510, 2019M650213).

## **Supporting Information**

The synthesis procedure, the original graph of Western blot and additional methods are available in Supporting Information

## References

- [1] Iranshahy M, Iranshahi M. Traditional uses, phytochemistry and pharmacology of asafoetida (*Ferula assa-foetida* oleo-gum-resin)-a review. *Journal of ethnopharmacology*. 2011;134(1):1-10.
- [2] Kleibl Z, Kristensen VN. Women at high risk of breast cancer: Molecular characteristics, clinical presentation and management. *Breast*. 2016;28:136-144.
- [3] Rogalska A, Miskiewicz K, Marczak A. Inhibitors of microtubule polymerization- new natural compounds as potential anti-cancer drugs. *Postepy higieny i medycyny doswiadczalnej*. 2015;69:571-585.
- [4] Jordan MA, Wilson L. Microtubules as a target for anticancer drugs. *Nature reviews. Cancer*. 2004;4(4):253-265.
- [5] Tangutur AD, Kumar D, Krishna KV, et al. Microtubule Targeting Agents as Cancer Chemotherapeutics: An Overview of Molecular Hybrids as Stabilizing and Destabilizing Agents. *Current topics in medicinal chemistry*. 2017;17(22):2523-2537.
- [6] Cosentino L, Redondo-Horcajo M, Zhao Y, et al. Synthesis and biological evaluation of colchicine B-ring analogues tethered with halogenated benzyl moieties. *Journal of medicinal chemistry*. 2012;55(24):11062-11066.
- [7] Cai D, Qiu Z, Yao W, et al. YSL-12, a novel microtubule-destabilizing agent, exerts potent anti-tumor activity against colon cancer in vitro and in vivo. *Cancer chemotherapy and pharmacology*. 2016;77(6):1217-1229.
- [8] Xu L, Wang W, Meng T, et al. New microtubulin inhibitor MT189 suppresses angiogenesis via the JNK-VEGF/VEGFR2 signaling axis. *Cancer letters*. 2018;416: 57-65.
- [9] Kochl R, Hu XW, Chan EY, et al. Microtubules facilitate autophagosome formation and fusion of autophagosomes with endosomes. *Traffic*. 2006;7(2):129-145.
- [10] Zhao PL, Li YH, Yang HK, et al. Design, synthesis and antiproliferative activity of novel 5-nitropyrimidine-2,4-diamine derivatives bearing alkyl acetate moiety. *European journal of medicinal chemistry*. 2016;118:161-169.

- [11] Meslamani J, Rognan D, Kellenberger E. sc-PDB: a database for identifying variations and multiplicity of 'druggable' binding sites in proteins. *Bioinformatics* 2011;27(9):1324-1326.
- [12] Protá AE, Danel F, Bachmann F, Bargsten K, Buey RM, Pohlmann J, *et al.* The novel microtubule-destabilizing drug BAL27862 binds to the colchicine site of tubulin with distinct effects on microtubule organization. *Journal of molecular biology* 2014;426(8):1848-1860.
- [13] Case DA, Cheatham TE, 3rd, Darden T, Gohlke H, Luo R, Merz KM, Jr., *et al.* The Amber biomolecular simulation programs. *Journal of computational chemistry* 2005;26(16):1668-1688.
- [14] Mei Y, Pan D, Jiang Y, Zhang W, Yao X, Dai Y, *et al.* Target discovery of chlorogenic acid derivatives from the flower buds of *Lonicera macranthoides* and their MAO B inhibitory mechanism. *Fitoterapia* 2019;134:297-304.
- [15] Shelanski ML, Gaskin F, Cantor CR. Microtubule assembly in the absence of added nucleotides. *Proc Natl Acad Sci U S A* 1973;70:765-8.
- [16] Martínez Molina D, Jafari R, Ignatushchenko M, Seki T, Larsson EA, Dan C, Sreekumar L, Cao Y, Nordlund P. Monitoring drug target engagement in cells and tissues using the cellular thermal shift assay. *Science*. 2013;341(6141):84-7.
- [17] Crowley LC, Marfell BJ, Waterhouse NJ. Detection of DNA Fragmentation in Apoptotic Cells by TUNEL. *Cold Spring Harbor protocols*. 2016.
- [18] Goulimari P, Kitzing TM, Knieling H, *et al.* Galpha12/13 is essential for directed cell migration and localized Rho-Dia1 function. *The Journal of biological chemistry*. 2005;280(51):42242-42251.
- [19] Zhang Z, Ren X, Lu X, *et al.* GZD856, a novel potent PDGFRalpha/beta inhibitor, suppresses the growth and migration of lung cancer cells in vitro and in vivo. *Cancer letters*. 2016;375(1):172-178.
- [20] Love MI, Huber W, Anders S. Moderated estimation of fold change and dispersion for RNA-seq data with DESeq2. *Genome biology*. 2014;15(12):550.
- [21] Lee A, Lee K, Kim D. Using reverse docking for target identification and its applications for drug discovery. *Expert opinion on drug discovery*. 2016;11(7):707-715.
- [22] Zimmermann S, Moelling K. Phosphorylation and regulation of Raf by Akt (protein kinase

- B). *Science*. 1999;286(5445):1741-1744.
- [23] Rommel C, Clarke BA, Zimmermann S, et al. Differentiation stage-specific inhibition of the Raf-MEK-ERK pathway by Akt. *Science*. 1999;286(5445):1738-1741.
- [24] Zhang J, Wang G, Zhou Y, et al. Mechanisms of autophagy and relevant small-molecule compounds for targeted cancer therapy. *Cellular and molecular life sciences*. 2018;75(10):1803-1826.
- [25] Yao D, Wang P, Zhang J, et al. Deconvoluting the relationships between autophagy and metastasis for potential cancer therapy. *Apoptosis*. 2016;21(6):683-698.
- [26] Zhang QC, Petrey D, Garzon JI, et al. PrePPI: a structure-informed database of protein-protein interactions. *Nucleic acids research*. 2013;41:D828-833.
- [27] Huang da W, Sherman BT, Lempicki RA. Systematic and integrative analysis of large gene lists using DAVID bioinformatics resources. *Nature protocols*. 2009;4(1):44-57.
- [28] Meng H, Li G, Huang J, et al. Sesquiterpene coumarin and sesquiterpene chromone derivatives from *Ferula ferulaeoides* (Steud.) Korov. *Fitoterapia*. 2013;86:70-77.
- [29] Kumar A, Sharma PR, Mondhe DM. Potential anticancer role of colchicine-based derivatives: an overview. *Anticancer Drugs*. 2017;28(3):250-262